Nanoparticle detection limits of TNO's Rapid Nano: modeling and experimental results

Peter van der Walle, Pragati Kumar, Dmitry Ityaksov, Richard Versluis, Diederik J. Maas, Olaf Kievit, Jochem Janssen, Jacques C.J. van der Donck
TNO, P.O. Box 155, 2600 AD, Delft, The Netherlands

ABSTRACT

TNO has developed the Rapid Nano scanner to detect nanoparticles on EUVL mask blanks. This scanner was designed to be used in particle qualifications of EUV reticle handling equipment. In this paper we present an end-to-end model of the Rapid Nano detection process. All important design parameters concerning illumination, detection and noise are included in the model. The prediction from the model matches the performance that was experimentally determined (59 nm LSE). The model will be used to design and predict the performance of future generations of particle scanners.

Keywords: particle inspection, EUV, qualification, detection limit, modeling, Rapid Nano, BRDF, speckle

1. INTRODUCTION

The lack of a suitable pellicle material for EUV lithography makes EUV reticles very sensitive to deposited particles. For this reason, EUV reticle handling equipment should have strict requirements on number of added particles per reticle pass (PRP). Before being taken into production, such equipment should undergo particle tests and qualification to show that the number of added particles (PRP) meets the requirements.

TNO has developed the Rapid Nano reticle blank scanner as a tool to aid in the particle qualification of reticle handling equipment [1-3]. Due to the very strict requirements on PRP, much tool-time is required on the equipment to be qualified [4]. The inspection equipment should add the minimum possible number of particles to the test blanks, as introducing extra background noise increases the required tool-time even more. The Rapid Nano was designed specifically with particle cleanliness in mind [5].

Here, we present an end-to-end model of the detection sensitivity of our scanner. The most important illumination, collection, substrate, particle and noise parameters are included in this model. The outcome of the model is a capture rate curve for a given particle type on a given substrate. The model correctly predicts the current performance and it can be used to make accurate predictions of future generations of the scanner.

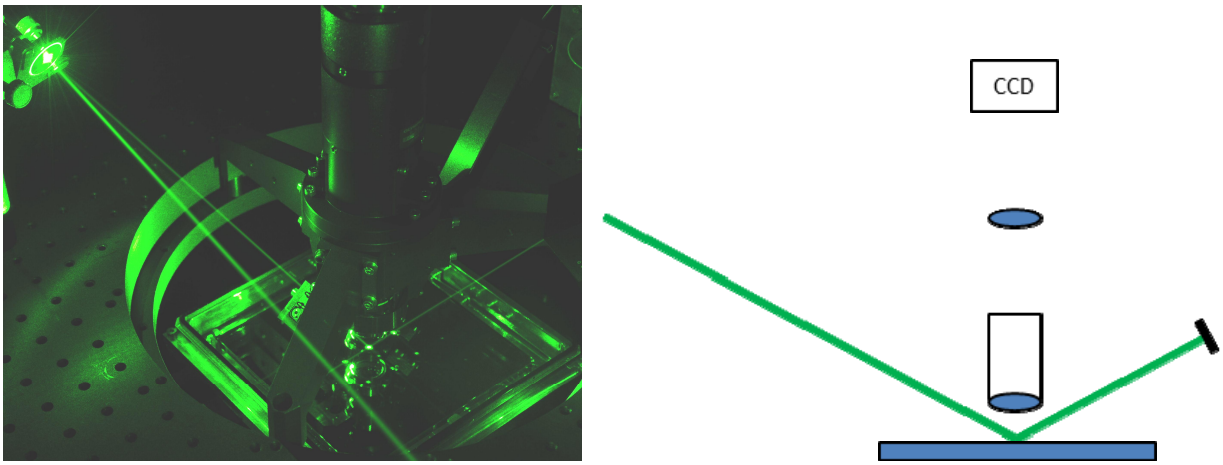

Figure 1: Photograph inside the Rapid Nano (left) and a schematic representation of the measurement principle (right).

Photomask Technology 2012, edited by Frank E. Abboud, Thomas B. Faure, Proc. of SPIE Vol. 8522, 85222Q · © 2012 SPIE · CCC code: 0277-786/12/$18 · doi: 10.1117/12.2006408

2. RAPID NANO

The detection method of the Rapid Nano particle scanner is based on dark-field microscopy as shown in Figure 1. The substrate is illuminated by a laser-beam under an angle outside the collection optics. The specular reflection is also outside the collection angle of the imaging optics and is absorbed in a beam-dump. An image of the illuminated area is projected on a CCD camera. In the case of a perfectly smooth substrate without particles, a completely dark image is collected. Particles will be visible in the image as a bright dots.

A complete mask blank can be inspected in a step-and-scan method. A total of 10.000 images cover a reticle surface. Image processing is performed on these images and the results are stitched together. The result is a particle map of the reticle blank. For equipment qualifications, a pre-map and post-map are required. Particles in the pre-map are subtracted from the post-map and the remaining particles are considered to be added by the handling equipment under test. The coordinates in the adder-map have sufficient accuracy for the particles to be found on an SEM, such that the source of the particle can be identified by determining its material composition using SEM-EDX.

3. MODELING

Our model determines the capture rate curve for a set of chosen system parameters. These parameters are listed in Table 1. The model first calculates the probability distribution of the gray value of a camera pixel. Two cases are considered, the gray value with background only (sections 3.1 and 3.2), and the gray value with a particle of a certain diameter present (section 3.5). Different sources of noise are included in the calculated distributions (section 3.3).

The background signal is caused by scattering on the surface roughness of the substrate. We are most interested in the limit of very small particles (<100 nm). In this limit, the size of the particle is much smaller than the size of the pixels. Therefore, the signal in the case that a particle is present can be described as the sum of the background signal and the light scattered by the particle.

Table 1: List of parameters included in the model.

Illumination	Incident elevation angle
	Polarization
	Wavelength
	Intensity
Imaging	Numerical Aperture (NA)
	Magnification
Camera	Quantum efficiency at wavelength
	Read-out noise
	Gain
	Pixel size
Substrate	Refractive index at wavelength
	Roughness PSD
Particle	Refractive index at wavelength
	Size

After calculating the probability distributions for a pixel with no particle and for pixels with particles of different sizes, the capture rate curve can be determined. First, a detection threshold is determined from the background distribution (section 3.4), after which the capture rate for each particle size is calculated by integrating the distributions from the threshold value to infinity (section 3.6).

3.1 Mean background signal

To be able to detect small particles, the blanks used in particle qualifications need to have a very smooth surface, with sub-nanometer root-mean square roughness. Scattering from such a smooth surface is well described by the Rayleigh-Rice perturbation theory, as the height variation on the substrate is much smaller than the inspection wavelength [6]. This theory relates the bi-directional reflectance distribution function (BRDF) of the substrate to the power spectral density (PSD) of the surface roughness. In this theory the surface is expressed as a superposition of 2D sinusoidal gratings and scattering is described as the first-order diffraction of the incident light on these gratings. The theory only yields the average scattering, while speckle effects are excluded. In the next section, we develop a description for the variance around this average background signal.

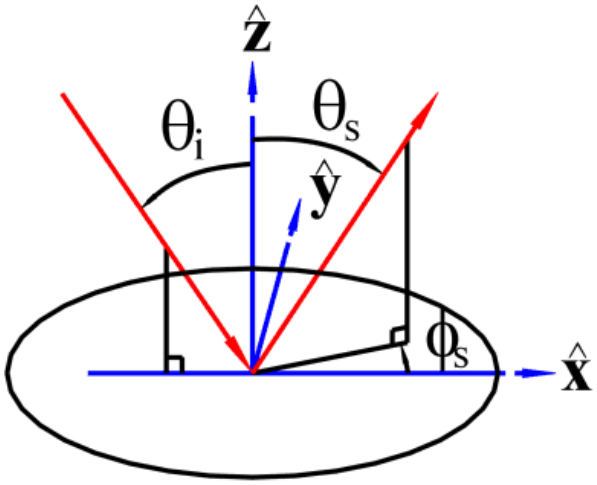

Figure 2: Coordinate system showing the definitions of incident elevation angle θ_i, scattered elevation angle θ_s and scattered azimuth angle ϕ_s.

The BRDF model provides a Jones matrix for scattering from an incident angle to a scattered angle. Because the system has cylindrical symmetry, only the elevation angle for the incident beam is specified, while for the scattered angle both the elevation and azimuth angle are specified (a schematic diagram is presented in Figure 2). The elements of the Jones matrix give the scattering amplitudes and phases for each combination of incident and scattered polarization (PP, PS, SP, SS) states. The total average background signal is calculated using the specified illumination angle and polarization, while integrating the scattering over all angles collected by the imaging system.

The model relies on a known 2D-PSD of the surface roughness of the substrate. This PSD can be measured using AFM or an optical surface-profiler. We determined the PSD of some of our substrates using AFM and using the measured values in the model shows that the calculated background scatter matches closely with the observed scatter. However, for some substrates surface roughness measurements were not available. For these substrates we used a fractal PSD model which describes the 2D-PSD as:

$$S_2 = A / f^C, \quad (1)$$

where A is the amplitude at unity spatial frequency, f is the spatial frequency and C is the slope at which the roughness drops-off towards higher spatial frequencies. We fixed C at a value of 2.8 and adjusted A to match the observed background scattering. This value for C is realistic for optically polished surfaces.

For the description of our background distribution not only its average value is needed, but also the variation around this value. Each diffraction angle collected by the imaging system is due to a different grating component on the surface. These gratings can be considered as having random amplitudes and random relative positions, which determine the relative phases between the diffraction angles. Thus, the background image is a Fourier-transform of a field with random amplitudes and phases. Mathematically this description is equivalent to a speckle pattern and its intensity distribution is well known to have an exponential probability distribution [7].

3.2 Variance of background signal

Looking at a typical background distribution recorded on the camera, as shown in Figure 3, we do not observe an exponential distribution. This difference is due to the finite size of the pixels of the camera. Each pixel integrates the intensity of a small area in the image space and therefore sums up the independent speckle contributions. The background distribution is well described by a gamma distribution. This distribution is the sum of a number of independent exponential distributions and can be defined by two parameters, k and ϕ. The parameter 'k' is the number of exponential distributions which are summed, while ϕ is the mean value of each exponential distribution. The mean of the total distribution is $k\phi$, while its variance is $k\phi^2$.

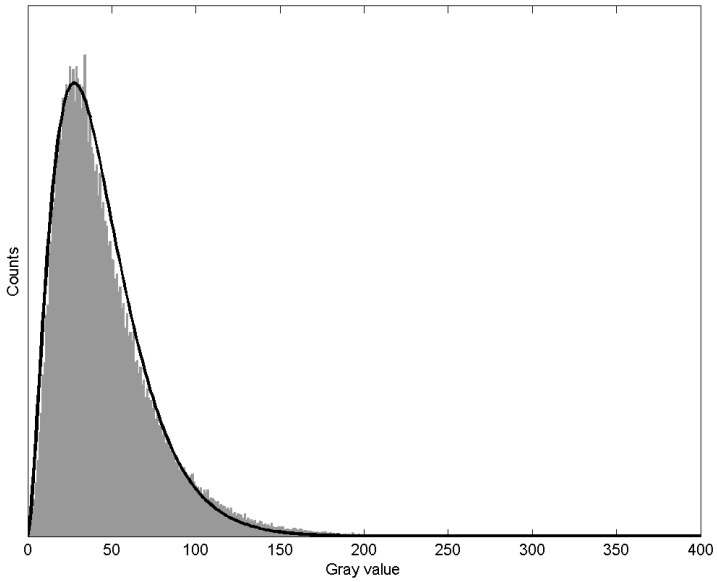

Figure 3: Typical distribution of the background signal (gray) and a gamma distribution with k = 2.7 and ϕ = 16.3.

The value of k depends on the typical size of a speckle with respect to the size of a pixel. The size of the speckles depends on the NA of the imaging optics, its magnification, and the wavelength of the light. We have performed a simple simulation of the described process. We take a 2d-array of values with normally distributed amplitudes and uniformly random phases. This array represents the amplitudes and phases of the scattered light in different diffraction angles. The number of values in this array is chosen such that at the end of this procedure, we end-up with 8x8 values in the calculated image within the size of a camera pixel. A circular aperture is applied to this array, which represents the imaging NA. All scattering angles not collected by the imaging optics are set to zero by this aperture. The Fourier-transform of the array is taken to calculate the field at the image position. This field is converted to the intensity of the image by taking the square magnitude. Finally, this image is binned into the camera pixels by summing blocks of 8x8 values. The values in the resulting image are distribution following a gamma distribution. The value of k can be determined from these statistics via $\text{mean}^2/\text{variance}$.

Performing this simulation with the experimental values, NA 0.42, wavelength 532 nm, magnification 9 and pixel size 7.4μm, we obtain a value for k of 2.7. A gamma distribution with this k-value matches well with the experimentally observed background histogram.

3.3 Noise

Noise is also considered and added to the calculated signal distributions. Two types of noise are taken into account in the model, the noise in the detection, and the noise due to the particle position on a finite size pixel. The detection noise is

further broken-down into count noise and read-out noise of the camera. These two noise sources can always be made negligible by collecting more light onto the camera at the cost of throughput.

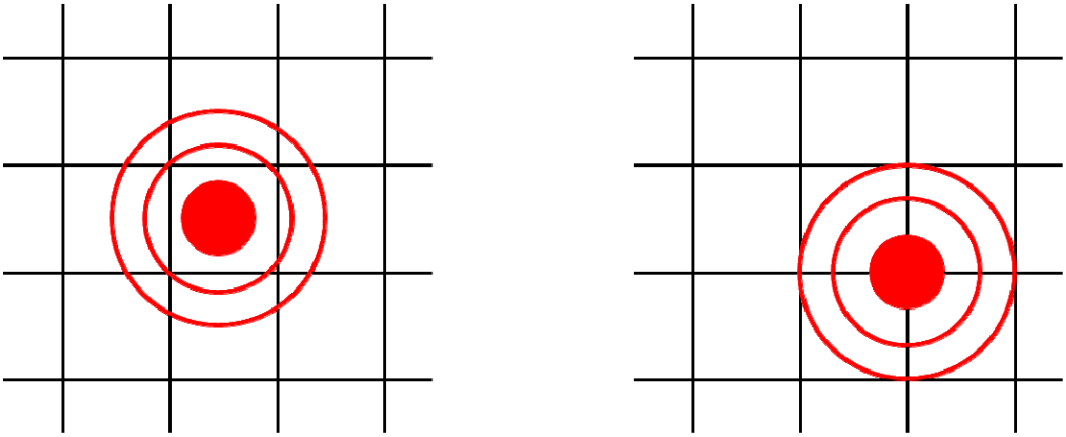

Figure 4: Two extreme cases for the position of the image of a particle on the pixel array. The situation on the left results in a high peak-value, while the situation on the left has a lower peak-value.

We use a simple threshold based detection method. When the gray-value of a pixel exceeds the threshold value, a particle is detected. The maximum pixel value generated by a particle depends on the relative position of the particle to the pixel array. When the particle is centered on a pixel the highest possible pixel value for this particle size occurs, while when the particle is positioned at the corner of four pixels, the lowest value is recorded, as shown in Figure 4. Depending on the ratio of pixel size to optical resolution, the difference between this maximum and minimum value can be large. We have estimated this noise source by integrating part of an Airy disk (at the optical resolution) over the size of a pixel. The pixel was shifted over the Airy disk to sample different possible particle positions. This sampling procedure results in a distribution for the maximum pixel value produced by a particle and is used in the calculation of the signal distribution for each particle size. This noise source can be reduced by taking a smaller pixel size relative to the optical resolution, but again at the cost of throughput.

3.4 Detection threshold

Now that we have a model for the background distribution, the detection threshold can be determined. When the background value, without any particle present, exceeds the threshold value, a false positive is detected. By using the predicted gamma distribution for the background signal, the expected number of false positives for a given threshold can be calculated. We chose the threshold value such that, with the total number of pixels on a substrate, less than one false positive is expected per scan [8]. A different number of acceptable false positives can be used with the detection threshold adjusted accordingly.

3.5 Particle signal

For the description of scattering by a particle, we used a model developed by Bobbert and Vlieger [9]. This model determines the BRDF for a sphere above a smooth substrate by solving Mie scattering and the Fresnel reflections self-consistently. We used a freely available implementation of this model in the SCATMECH library [10]. This library was also used for the scattering from the bare substrate.

The parameters for the model are the substrate refractive index, particle refractive index, particle diameter, polarization state and the wavelength of illumination. An optional parameter is the distance between particle and substrate. We have only considered the case where the particle is touching the substrate. Other optional parameters are a stack of coatings on the substrate and a coating on the particle.

In the same way as in the roughness BRDF model, the BV-model provides a Jones matrix for an incident elevation angle, a scattered elevation and azimuth angle. With the Jones matrix, the scattering intensity for the chosen incident polarization state is calculated. Also here the incident angle is fixed and the scattering angle is integrated over the NA of the imaging optics.

The previously determined distribution for the maximum pixel value is multiplied by the calculated particle scattering intensity. The resulting distribution is convolved with the background distribution to represent the distribution for the sum of both contributions.

3.6 Capture rate curve

A particle is detected when the maximum pixel value it produces is larger than the determined threshold. Therefore the capture rate of a particle is just the integral of the entire probability distribution above the threshold. We determine the probability distributions for a number of different particle sizes and integrate them to arrive at their capture rate. Such capture rate curves are shown in Figure 5 for a number of different particle materials. The system configuration for this calculation was the current Rapid Nano particle scanner and as the substrate a polished silicon wafer. We specify the lower detection limit of our scanner at the point where the capture rate is 95% for a PSL particle. The abbreviation LSE for latex sphere equivalent is used to indicate this reference particle.

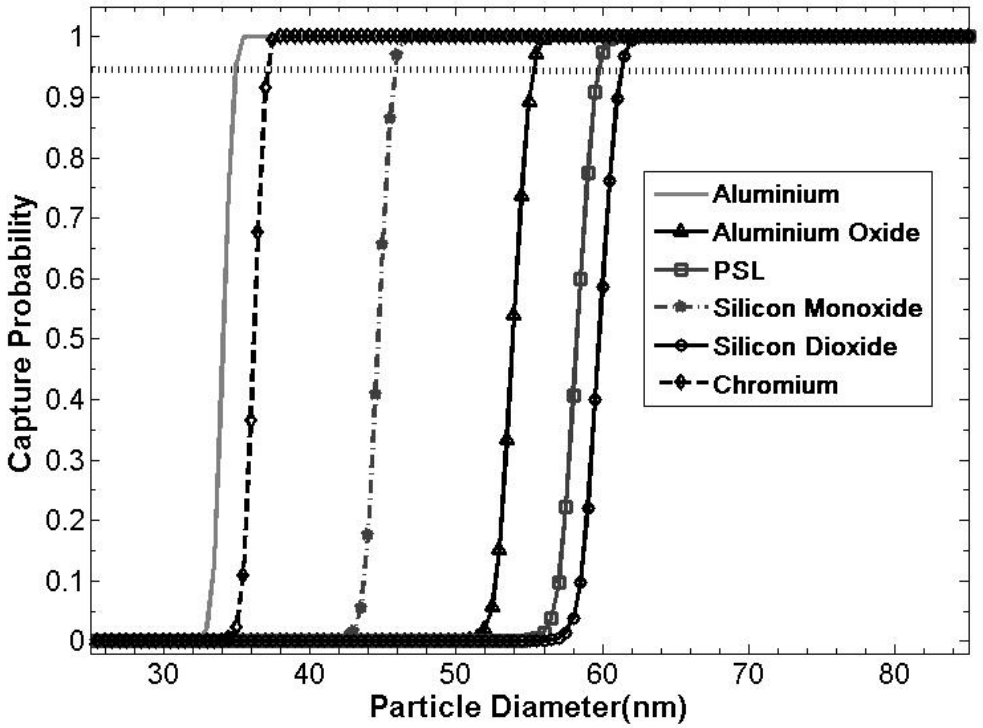

Figure 5: Model output for different particle materials on a polished silicon wafer, using the current generation illumination and detection parameters.

For the current system, the predicted performance is 59 nm LSE. The parameter, with the strongest influence on the sensitivity, is the illumination wavelength. By using a shorter wavelength, higher spatial frequencies of the substrate roughness are sampled. The roughness at higher frequencies is generally less than at lower frequencies. Therefore the signal to background ratio increases by using a shorter wavelength. When the PSD of the roughness can be described by the fractal model (equation 1), this ratio scales as $1/\lambda^C$. The model prediction for a system using 266 nm light and an optimized illumination mode is a sensitivity of 20 nm LSE on polished silicon wafers.

4. EXPERIMENTAL

The capture rate curve of the current Rapid Nano system with 532 nm illumination was determined experimentally. The procedure outlined in the SEMI M50 standard [8] was followed. First, the scanner was calibrated using samples with known particle sizes. Samples were produced by spin-coating a diluted solution of PSL particles on a 100 mm silicon wafer. Particle sizes of 60, 80 and 100 nm were used.

The calibration samples were inspected with the scanner and histograms of the detection intensities were made. The signals at the peak of each histogram were assigned the to the corresponding particle size. A curve was fit through the three points, while ensuring that the extrapolation towards smaller particles scaled as diameter to the power 6. This extrapolation is supported by the model calculations.

An area on the sample with particles around 60 nm in diameter was inspected 30 times, resulting in 30 particle maps with a size plus x and y coordinate for each detection. The 30 maps were matched on particle positions. Any particle detected within a radius of 6 μm was considered to be the same particle. The choice of the radius did not have a significant effect on the final result. The capture rate of each individual particle was determined as the number of scans it was present divided by the total number of scans. Finally, the particles were put into bins according to the average size they were detected at and the average capture rate per bin was determined. The result is shown in Figure 6. The particle size for which the capture rate is 95 % is 59 nm, which corresponds exactly to the value predicted by the model.

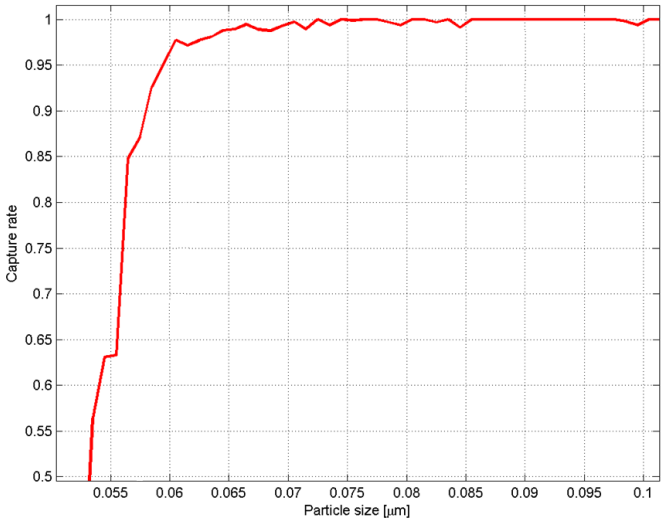

Figure 6: Experimental capture rate curve, determined by repeated scanning of a substrate with PSL particles around 60 nm deposited.

5. CONCLUSION

An end-to-end model of the Rapid Nano particle scanner has been developed. A large number of design parameters that influence the performance are included in the model, such as illumination and collection geometry, and camera noise. In addition, the substrate roughness and material are included. The model predicts the performance of the Rapid Nano scanner at 59 nm LSE on polished silicon wafers.

An important intermediate result of the model is the description of the background signal. The model predicts the probability distribution for this signal, using the substrate roughness and collection geometry. This predicted probability distribution matches well with the experimentally observed distribution.

The performance of the scanner was also determined experimentally, using PSL spheres of calibrated sizes. The experimentally determined performance matches the model prediction. This result validates the output of our model. The model will be used as a tool in the design of future generations of the Rapid Nano particle scanner down to a sensitivity of 20 nm LSE.

REFERENCES

[1] Donck, J.C.J. van der, Snel, R., Stortelder, J.K., Abutan, A., Oostrom, S., Reek, S. van, Zwan, B. van der, Walle, P. van der, "Particle detection on flat surfaces", Proc. SPIE 7969, 1S (2011).

[2] Stortelder, J.K., Donck, J.C.J. van der, Oostrom, S., Walle, P. van der, Dress, P., Brux, O., "Particle qualification procedure for the TNO EUV reticle load port module of the HamaTech MaskTrackPro cleaning tool", Proc. SPIE 7969, 1Q (2011).

[3] Brux, O., Walle, P. van der, Donck, J.C.J. van der, Dress, P., "Investigating the intrinsic cleanliness of automated handling designed for EUV mask pod-in-pod systems", Proc. SPIE 8166, 2S (2011).

[4] Donck, J.C.J. van der, Stortelder, J.K., Derksen, G.B., "Optimized qualification protocol on particle cleanliness for EUV mask infrastructure", Proc. SPIE 8166, 2T (2011).

[5] Heerens, G.J., "Container for a mask", EP1434094A1 (2004).

[6] Church, E.L., Takacs, P.Z., "Surface scattering", Handbook of Optics (Volume I), Chapter 7 (2009).

[7] Goodman, J.W., "Some fundamental properties of speckle", JOSA 66, 1145-1150 (1976).

[8] "Test methods for determining capture rate and false count rate for surface scanning inspection systems by the overlay method", SEMI M50-0307 (2007).

[9] Bobbert, P.A., Vlieger, J., "Light scattering by a sphere on a substrate", Physica 137A, 209-242 (1986).

[10] Germer, T.A., "SCATMECH: Polarized Light Scattering C++ Class Library", version 6.0.1, (available at http://physics.nist.gov/scatmech).